Available online at www.sciencedirect.com
ScienceDirect
Biochimica et Biophysica Acta 1778 (2008) 945–953
Biochimica et Biophysica Acta BBA
www.elsevier.com/locate/bbamem

Membrane curvature and surface area per lipid affect the conformation and oligomeric state of HIV-1 fusion peptide: A combined FTIR and MD simulation study

Bogdan Barz [a], Tuck C. Wong [b,1], Ioan Kosztin [a,*]

[a] Department of Physics and Astronomy, University of Missouri-Columbia, Columbia, MO 65211, USA
[b] Department of Chemistry, University of Missouri-Columbia, Columbia, MO 65211, USA

Received 3 August 2007; received in revised form 19 November 2007; accepted 21 November 2007
Available online 14 December 2007

Abstract

Fourier-transformed infrared spectroscopy (FTIR) and molecular dynamics (MD) simulation results are presented to support our hypothesis that the conformation and the oligomeric state of the HIV-1 gp41 fusion domain or fusion peptide (gp41-FP) are determined by the membrane surface area per lipid (APL), which is affected by the membrane curvature. FTIR of the gp41-FP in the Aerosol-OT (AOT) reversed micellar system showed that as APL decreases from ~50 to 35 Å^2 by varying the AOT/water ratio, the FP changes from the monomeric α-helical to the oligomeric β-sheet structure. MD simulations in POPE lipid bilayer systems showed that as the APL decreases by applying a negative surface tension, helical monomers start to unfold into turn-like structures. Furthermore, an increase in the applied lateral pressure during nonequilibrium MD simulations favored the formation of β-sheet structure. These results provide better insight into the relationship between the structures of the gp41-FP and the membrane, which is essential in understanding the membrane fusion process. The implication of the results of this work on what is the fusogenic structure of the HIV-1 FP is discussed.

Keywords: HIV; gp41 fusion peptide; Membrane fusion; Conformation; Fourier-transformed infrared spectroscopy (FTIR); Molecular dynamics (MD) simulation

1. Introduction

Enveloped viruses such as human immunodeficiency virus (HIV) and influenza virus infect their target cells by a process involving cell-specific binding to the cell membrane followed by fusion of the viral enveloped membrane with cellular membranes [1]. The enveloped viral protein (fusion protein) is responsible for the actual membrane fusion step, leading to the release of viral contents into the target cell and subsequent infection. For many viruses, a small segment of the fusion protein usually located at the N-terminus is responsible for the early stage in the membrane fusion process [2]. This domain is usually referred to as the fusion domain or fusion peptide (FP). In the case of HIV type 1 (HIV-1), the envelope glycoprotein gp160 contains two non-covalently associated subunits, gp120 and gp41 [1]. The subunit gp120 contains sites for viral binding to target cells containing CD4 [3] and chemokine coreceptors, primarily CCR5 or CXCR4 [4–7], while the transmembrane subunit, gp41, is responsible for the membrane fusion process [8]. The viral glycoproteins are assembled as coiled-coil homotrimers [2,9–18]. The N-terminal gp41-FP is highly homologous with corresponding domains of other enveloped viruses [19], and its first 16 residues (AVGIGALFLGFLGAAG) are mostly hydrophobic.

Strong evidence coming from mutagenesis studies of intact enveloped proteins as well as from synthetic FPs implicates the role of the FP domain in mediating membrane fusion [20–23]. Synthetic peptides mimicking the N-terminal gp41-FP have also been shown to cause lipid mixing and membrane fusion [24–30]. Therefore, structural studies have utilized the synthetic FP solubilized in lipid micelles or reconstituted in lipid bilayers to gain insight into the structural requirements for viral fusion activities. A variety of experimental methods (NMR, FTIR, CD, ESR) as well as molecular dynamics (MD) simulations has been

* Corresponding author. Tel.: +1 573 882 7241; fax: +1 573 882 4195.
E-mail addresses: WongT@missouri.edu (T.C. Wong), KosztinI@missouri.edu (I. Kosztin).
[1] Tel.: +1 573 882 7725; fax: +1 573 882 2754.

0005-2736/$ - see front matter © 2007 Elsevier B.V. All rights reserved.
doi:10.1016/j.bbamem.2007.11.014

used to study the structure of the FPs and the mode of interaction with the membrane. Studies to date have shown that both gp41-FP and the influenza HA_2 FP display considerable structural plasticity. It can adopt either the monomeric α-helical or the oligomeric β-sheet conformations. While shorter, 16- or 23-residues, gp41-FPs have been found to be in both α-helical or the oligomeric β-sheet conformations, longer constructs (such as the 70-residue peptide) which include hydrophilic amino acids or the whole N-heptad repeats showed only a highly fusogenic β-sheet structure [31,32]. For shorter FPs (16- or 23-residues), a consensus has been reached that at higher peptide loading, i.e., lower [Lipid]/[Peptide] ratio ([L]/[P]), the oligomeric β-sheet is favored, while at higher [L]/[P], monomeric α-helical form dominates. However, even at comparable [L]/[P] in different membrane mimics, a variety of results were obtained. For example, all experiments of the FP in micelles revealed predominantly α-helical structure, at [L]/[P] typically from 100 to 50 [33–38]. On the other hand, for the same range of [L]/[P] values in lipid bilayers, both the α-helical and β-sheet structures or their mixture were observed due to an increase of percentage of β-sheet structure at the expense of the α-helical one [39], suggesting that the curvature of the membrane has an effect on the oligomeric and conformational state of the FP. In general, the membrane surface area, or area per lipid (APL), is higher in micelles than in bilayers because of the positive curvature in the micellar surface. At the same time, previous investigations have demonstrated that the conformation and oligomeric state of the gp41-FP can be altered by changing the APL while, apparently, keeping the membrane curvature intact. For example, Nieva et al. observed that, at [L]/[P] of 75 and 100, α to β transition in the gp41-FP in 1-palmitoyl-2-oleoylphosphatidylglycerol (POPG) large unilamellar vesicles (LUV) occurred upon the addition of 5 mM Ca^{++} ions [31,40]. Addition of cations, especially divalent cations, usually causes a decrease in the APL of lipid bilayers or monolayers with negatively charged headgroups (although Ca^{++} ions can change the intrinsic membrane curvature of certain negatively charged lipid systems and the hydration state of these lipids). For example, Demel et al. [41] showed that the addition of Ca^{++} ions causes a decrease of 5–9 $Å^2$ in 1,2-dipalmoitoy-*sn*-glycerol-3-phosphoserine (DPPS) monolayer. Similarly, Castano and Desbat reported that α to β transition in FP in a DOPC/Cholesterol/DOPE/DOPG (6/5/3/2) monolayer took place at [L]/[P] = 10 upon application of lateral compression of the monolayer [39]. However, their study was conducted at a much lower [L]/[P] ratio, and alternative interpretation of the cause for the observation, such as the FP getting squeezed out of the monolayer by high pressure and aggregate to β-sheet structure, is conceivable. Combining the results of these two lines of studies – the effects of curvature change and the effects of APL change that may not involve changes in curvature – leads us to believe that a decrease in the APL either by changing the curvature of the membrane or by other means, e. g., by applying lateral compression or addition of cations, results in a shift from monomeric α-helical to oligomeric β-sheet structures. Thus we propose that the conformation and the oligomeric state of the gp41-FP are determined by the APL and the effect of the curvature of the membrane surface on the conformation of the gp41-FP is mainly manifested through the induced change in the APL. Although the effects of APL on the conformation of the FP have been alluded to in the past (e. g., Refs. [31,39]), they have not been systematically studied nor clearly advocated. To test this hypothesis, we have chosen the reversed micellar system formed by Aerosol-OT (AOT, sodium dioctyl sulfosuccinate) as the membrane mimicking system. Although reversed micelles have seldom been used in the studies of the interactions of the FP with membrane mimics, there are compelling rationales for choosing the AOT reversed micelles for the present purpose. First, the AOT reversed micelles provide a water/lipid interface with negative curvature, and with APL ranging from as low as 30 to about 50 $Å^2$ [42], a range substantially lower than the membrane models used by previous studies, typically of 60–80 $Å^2$ for planar bilayer surfaces and for micellar surfaces with positive curvature. The use of the reverse micelles adds membrane surface with negative curvature as mimics, which has not been used in the past in the studies of the conformation and membrane interaction for FPs, and it drastically extends the range of APL for our study to adequately test our hypothesis. Second, the reversed micellar system offers a system where the membrane curvature, and thus the APL, can be fine-tuned by varying the water/lipid ratio (W_o = [water]/[AOT]) [42]. Since the APL is a more quantifiable parameter than the curvature, we will present the results and discussion in terms of the variation in APL. It should be born in mind, however, that the changes in APL are the result of changes in the curvature of the membrane surface.

In this paper we report results from Fourier-transformed infrared spectroscopy (FTIR) measurements and from all atom molecular dynamics (MD) simulations, which taken together validate our hypothesis that the conformation and the oligomeric state of the HIV-1 gp41-FP are determined by the APL. FTIR was used to determine the conformational state of the fusion peptide in AOT reversed micelles over a range of water/lipid ratio values corresponding to a variation of the APL from small (~35 $Å^2$) to intermediate (~50 $Å^2$) values. The conformational information from FTIR spectra is readily available by analyzing the amide-I band (1600–1700 cm^{-1}) region. Furthermore, the IR time scale is faster than that of NMR and as a result, different conformational states, rather than a time-average over these states, can be determined from the IR spectra. The MD simulations of gp41-FP dimers in solvated lipid bilayers reported here were designed to investigate their transition from α-helical to β-sheet conformations as a result of the decrease of the APL. The main aim of these simulations was not to corroborate the findings of our FTIR experiments but rather to directly look at the effects of APL changes on conformations of the FP and to complement the FTIR findings by focusing on the APL region (i.e., from 50 to 70 $Å^2$) that is not accessible in the AOT reversed micelles.

2. Materials and methods

2.1. Fourier-transformed infrared spectroscopy

A liquid IR cell with CaF_2 windows and 15 μM path length was used. Infrared spectra were taken on a Thermal-Nicolet Nexus 670 Spectrometer with a deuterated triglyceride sulfate (DTGS) detector at room temperature (~25 °C).

For each spectrum, 1024 scans were obtained at 2 cm^{-1} resolution from 400–4000 cm^{-1}. The solvent spectrum was taken under identical conditions and was subtracted from the spectrum of each sample.

A stock solution of 1 M AOT (Aldrich, 98%) in octane (Mallinkrodt, 99+%) was prepared. Appropriate amount of D_2O (Cambridge Isotope laboratory, 99.9%) was added to a portion of the stock solution to make the AOT/D_2O/octane reversed micelles at various W_o values. The 23-residue N-terminal FP (AVGIGALFLGFLGAAGSTMGARS-NH_2, FP23) was synthesized and purified by the University of Missouri Peptide Synthesis Core (purity>90%) and lyophilized to remove trifluoroacetate (TFA) counterions. However, a small amount of TFA ions remained in the sample. By using ^{19}F NMR and comparing with a TFA solution of known concentration, it can be determined that there is less than one TFA ion per peptide. Nevertheless, a peak at 1674 cm^{-1} arising from TFA was observed in the FTIR spectra. Fortunately, there is usually no signal from the FP in this region of the spectrum and thus the TFA signal does not mask the important signals from the helical and, especially, the β-sheet structures. A weighted amount of FP23 was then dissolved in the reversed micellar solution and the resulting sample was allowed to equilibrate for at least 24 h to ensure complete exchange of the amide protons by deuterium. The lipid/peptide ratio ([L]/[P]) for each sample was kept at 500, corresponding to very low peptide loading. By keeping a constant [L]/[P] ratio, the amount of FP in each sample for W_o=5, 7.5 and 10 varied slightly since the amount of AOT decreases as W_o decreases (by about 8% from W_o=5 to W_o=10). This [L]/[P] value of 500 was definitely not maintained at W_o=18, as the solubility of the peptide in the reversed micelles decreases drastically at this high W_o value. By recovering the undissolved FP23, it was estimated that only about 30±10% of the FP intended to keep [L]/[P] at 500 was dissolved in the reversed micelles. Thus, in fact the [L]/[P] for the sample at W_o=18 is well over 1000, and because of the much reduced solubility of FP23 no spectrum was obtained for W_o>18.

2.2. Molecular dynamics

To investigate the APL dependence of the conformational state and stability of the gp41-FP by means of MD simulations we have built three model systems, referred to as A1, A2 and B, starting from its all atom structure obtained from FTIR spectroscopy (PDB entry code 1ERF [37]) and employing the molecular modeling and visualization program VMD [43]. After completing the MD simulations reported here, two higher resolution NMR structures of HIV-1 gp41 became available in the PDB (entry codes 2ARI [36], and 2PJV [38]). The small RMSD between the helical region of 1ERF and 2ARI, along with the stability of the structure 1ERF during our several ns long MD trajectories lead us to believe that the MD simulation results reported in the present work are robust and should be reproducible by using the new higher resolution structures. Each system consisted of a gp41-FP dimer inserted in a fully solvated bilayer of palmitoyloleoylphosphatidylethanolamine (POPE) lipid molecules. In A1 and A2 the dimer was constructed by duplicating the structure of the 23-residue-long α-helical FP. The N-termini of the monomers were protonated and the axes of the α-helices (residues 4 to 12) in each dimer were oriented parallel with each other and separated by 5 Å. By using the NAMD Energy plugin of VMD, the relative angular orientation of the monomers with respect to their parallel axes was determined such that it minimized in vacuum the interaction energy between them. For A1 (A2) the Membrane plugin of VMD was used to insert the α-helical dimer perpendicular (parallel) to the surface of a preequilibrated rectangular patch of POPE membrane bilayer with solvated lipid headgroups. In both systems the disordered polar C-termini (residues 17 to 23) of the dimers were kept outside the membrane during the insertion process. Lipid molecules within 0.6 Å of the proteins were removed. Next, the membrane–peptide complexes were solvated by adding two 15 Å thick layers of water to each side of the membrane by using the VMD plugin Solvate. Water molecules trapped in the hydrophobic region of the membrane were removed. Finally, the VMD plugin Autoionize was employed to place at energetically favorable positions 4 Cl^- ions to restore the electro-neutrality of the systems. The resulting system A1 (A2) shown in Fig. 1a–b (Fig. 1c–d) had a total of 26,608 (35,038) atoms, containing 4414 (6349) water molecules, 48 (58) lipid molecules in the membrane leaflet that contained the α-dimer and 54 (65) in other leaflet.

In model system B the gp41-FP dimer was prepared in an elongated β-conformation as opposed to the α-conformation used in A1 and A2. This was achieved by stretching in vacuum the N-terminal fusion domain (residues 1 to 16) of each monomer in system A2 from the initial length of ~23 Å to 47 Å by means of interactive molecular dynamics [44]. In building system B the insertion of the β-dimer into the POPE membrane and the subsequent solvation followed the same protocol as for system A2. The final system B shown in Fig. 1e–f had 34,573 atoms, with 6194 water molecules and 58 (65) lipid molecules in the membrane leaflet with (without) the β-dimer.

All MD simulations were preformed with the program NAMD-2.5 [45] by using the CHARMM27 force field parameters for proteins [46,47] and lipids [48]. Water molecules were modeled as TIP3P [49]. The non-bonded van der Waals interactions were cut off at 12 Å, with smooth switching function starting at 10 Å. Long range electrostatic interactions were treated without cut off by employing the PME method [50]. An integration timestep of 2 fs was employed in all simulations by using the SHAKE constraint on all hydrogen atoms [51]. Unless otherwise stated, all simulations were carried out in the NpT ensemble [52] under normal conditions (T=300 K and $p=10^5$ Pa). Langevin dynamics, with a damping coefficient of 5 ps^{-1}, was used to keep the temperature constant. The hybrid Nose–Hoover Langevin piston method, with the same decay period and damping time of 100 fs, was employed to maintain a constant pressure. In order to minimize finite size effects periodic boundary conditions with flexible cell were used.

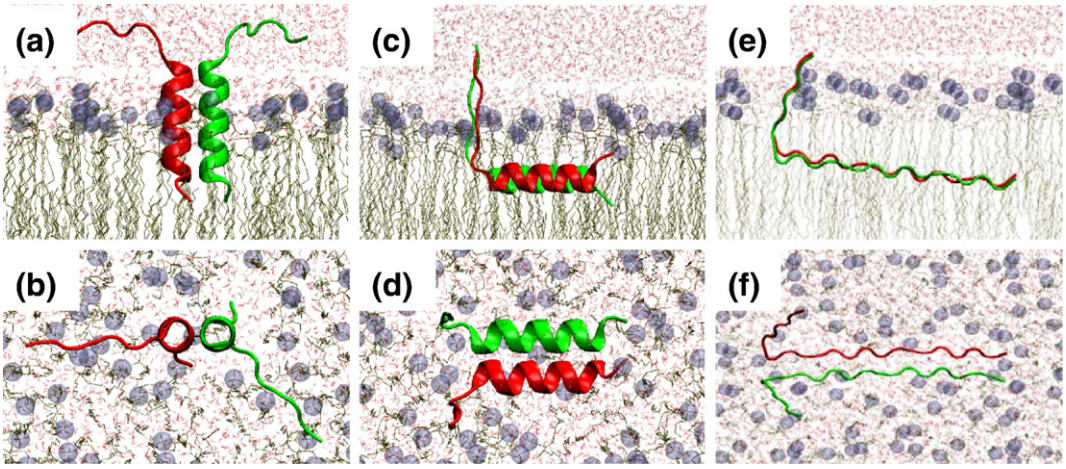

Fig. 1. (a) Side and (b) top views of the α-helical gp41-FP dimer inserted perpendicular into the upper leaflet of a POPE lipid bilayer (system A1). The peptides are shown in cartoon representation, the phosphorous atoms of the lipid headgroups are shown in van der Waals representation while the rest of the lipid molecules and the solvent water molecules are shown in line representation. Similarly, side and top views of the gp41-FP dimers in α-helical (system A2) and β-sheet (system B) conformations inserted into the POPE lipid bilayer parallel to its surface are shown in (c), (e) and (d), (f), respectively. (Images rendered with VMD [43].)

Energy minimization and equilibration of the systems were carried out in several stages. First, the systems were subjected to 3×10^4 minimization steps by harmonically restraining the C_α atoms of the proteins and the position of the phosphorous atoms of the lipid headgroups along the normal direction to the surface of the membrane. Next, the systems were brought to room temperature by gradual heating during a 0.5 ns period. Finally, after removing all the restraints, 2 ns (4 ns in case of system A1) long free equilibrations in the NpT ensemble were carried out for each system. The area of the membrane was kept constant for A1 and B but allowed to vary for A2. The sizes of the unit cell corresponding to the built (equilibrated) systems A1, A2 and B were $61\times61\times81$ Å^3 ($61\times61\times69$ Å^3), $71\times61\times88$ Å^3 ($71\times55\times85$ Å^3), and $56\times86\times83$ Å^3 ($56\times86\times69$ Å^3), respectively.

A set of five MD simulations in the NpT ensemble, referred to as S1, …, S5, were performed using the equilibrated systems A1, A2 and B. The 30 ns long simulations S1 and S2 were designed to test the stability of the α-helical conformation of the gp41-FP monomers in system A1 against helix–coil transition triggered by the variation of APL. While in S1 the membrane area was kept fixed, corresponding to APL ≈ 70 Å^2, in S2 the membrane area was increased (or equivalently APL decreased) in time through the application of a negative surface tension $\sigma=-50$ mN/m by setting $p_x=p_y=p_z-\sigma/\ell_z$, with $p_i=10^5$ Pa, ($i=x,y,z$), the diagonal elements of the pressure tensor [52,53], and ℓ_z the length of the unit cell along the z-direction perpendicular on the surface of the membrane.

The purpose of simulations S3 and S4 of system A2 was to investigate the APL dependence of the transformation of the α-helical gp41-FP monomers into turns followed by the formation of β-bridges as precursors of the dimer in the β-sheet conformation. Since the time scales on which lipid molecules undergo lateral diffusion in the membrane and monomeric α-helical gp41-FPs unfold within the membrane are orders of magnitude larger than the longest equilibrium MD simulations (~100 ns), we have resorted to nonequilibrium *steered molecular dynamics* (SMD) simulations in which properly chosen external forces are applied to the biomolecular system in order to speed up processes of interest [54]. In the 5 ns long SMD simulations S3 and S4 the forced unfolding of the α-helical gp41-FP monomers (system A2) was brought about by pulling apart the C_α atoms of residues 1 and 16 through a spring (elastic constant $k=1$ nN/Å) inserted between them, whose undeformed length was increased uniformly from 24 Å to 47 Å, which corresponds to the length of a monomer in the β-structure configuration. In S4 the reduction of the APL was mimicked by applying an attractive force $F_0=109$ pN/C_α atom (turned on gradually during the first 1.5 ns of the SMD simulation) between the gp41-FP monomers. No such confining force was applied during S3.

Finally, the purpose of the 15 ns long equilibrium MD simulation S5, corresponding to APL = 74 Å^2, was to investigate the conformational stability of the β-sheet gp41-FP dimer (system B), and to compare this with the unfolded structure of A2 at the end of the SMD simulations S3 and S4.

3. Results

3.1. Fourier-transformed infrared spectroscopy

The FTIR spectra of the FP23/AOT reversed micelle sample in the 1600–1700 cm^{-1} region at W_o values ranging from 5 to 18 are shown in Fig. 2. Also shown in Fig. 2 is the variation of the APL (in Å^2) as a function of W_o. At high value of $W_o=18$, corresponding to an APL of ~51 Å^2 [42], the quality of the spectrum was quite poor (Fig. 2D), due to the substantially lower solubility of the FP in the AOT reverse micelles of this composition. A single peak at 1674 cm^{-1} was observed (Fig. 2D). As indicated in the previous section, this peak is due to the residual TFA in the sample. On the low frequency side of the TFA signal, additional signal is evident. By deconvolution of the spectral lines, a broad signal centered around 1650 cm^{-1} was found. This signal is commonly assigned to α-helical and random coil structures [55]. Unfortunately it is not easy to distinguish these two structures.

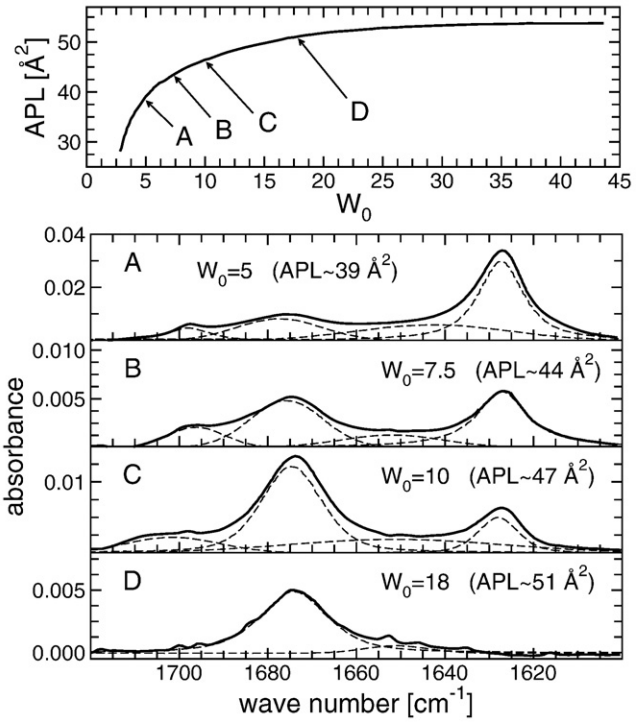

Fig. 2. Top panel: Area per lipid (APL) as a function of the water/lipid ratio (W_o). Lower panels A–D: The amide-I region (1600–1700 cm^{-1}) of the FTIR spectrum (solid curve) of gp41-FP in the AOT reversed micelles corresponding to W_o values indicated by arrows in the top panel. The dashed curves represent the deconvoluted FTIR bands described in the text.

Due to the low intensity and the broadness of this peak, it is also conceivable that it could have arisen from an artifact due to incomplete subtraction of the background signal. As W_o, and APL, decrease, another peak at 1627 cm^{-1} appeared (Fig. 2A–C). The intensity of the peak at 1627 cm^{-1} was found to increase relative to the TFA peak at 1674 cm^{-1} as W_o decreases. At the lowest W_o value of 5 in this study, the peak at 1627 cm^{-1} completely dominates (Fig. 2A). Strictly speaking, the intensities of the peak at each wavenumber (1674 and 1627 cm^{-1}) cannot be compared directly between spectra because of changes in concentration—the amount of peptide in the sample is smaller at higher W_o. The amount of FP in the sample cell decreases by ~8% from $W_o=5$ to $W_o=10$, but becomes a particular problem for the sample at $W_o=18$, where the FP concentration is substantially lower because of the drastically reduced solubility. Thus the intensities of the signal in Fig. 2D are substantially weaker than the rest of the spectra. Nevertheless, it is unmistakable that the intensity of the peak at 1627 cm^{-1} increases significantly (relative to the TFA peak and to the broad signal centered around 1650 cm^{-1}) as W_o decreases.

The 1627 cm^{-1} signal is commonly assigned to the anti-parallel β-sheet structure [39]. At the low peptide loading ([L]/[P] = 500) that was used in this work, and even at higher peptide loading (e. g. [L]/[P] ~ 100) α-helical structure was usually found to dominate, definitely in micelles [33–36], and even in bilayers and monolayers (APL of 60 Å^2 or higher). We believed that when the APL has decreased below 50 Å^2 ($W_o<18$ in the AOT system) the lateral compression causes the α-helical monomers

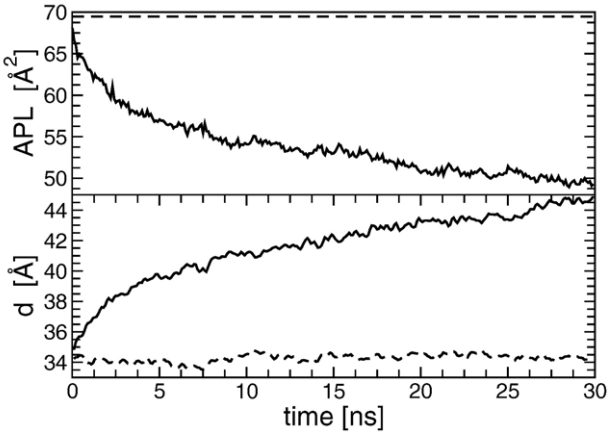

Fig. 3. Time evolution of APL (top panel) and of the lipid bilayer thickness (bottom panel) during MD simulations S1 (dashed line) and S2 (solid line) of system A1 described in the text.

to unfold into turn-structures (as supported by MD results discussed in the next section), and then the monomers in the transient turn-structures aggregate and form β-sheets. The oligomeric β-sheet structure ultimately becomes the dominant form at the lowest end of the APL range of our study. The approximate values for the ratios of the intensities of the β-sheet/(α-helical+random coil) are 1.6, 1.5 and 0.45 for W_o=5, 7.5 and 10, respectively (Fig. 2), while at W_o=18, no β-sheet signal was observed. Bear in mind that these numbers are highly qualitative. Thus the results support our hypothesis that the APL determines the oligomeric state and the conformation of the gp41-FP. The monomeric α-helical conformers of the FP turn increasingly into oligomeric β-sheet structure as APL decreases. Whether α to β transition was observed in this study involving the chosen range of low APL is not as clear-cut as we would like it to be. However, even if the broad signal at 1650 cm^{-1} does not arise from the α-helical structure but rather from an artifact, this may simply mean that at this range of low APL value, α-helical structure no longer exists. It must be emphasized that as W_o decreases, it is unmistakable that the signal corresponding to the β-sheet structure becomes more dominant relative to both the TFA signal and to the putative α-helical signal. Since the only source of TFA was from the peptide, the TFA signal serves as a reliable internal standard that clearly showed the growth of the β-sheet signal as W_o (and the APL) decreases. And thus the β-sheet structure is preferred at low APL, consistent with our hypothesis.

3.2. Molecular dynamics

Throughout the simulations, due to the strong electrostatic interaction between their protonated N-termini and the negatively charged phosphate groups, the monomers remained in close proximity to the surface of the membrane. In case of system A1, where the α-helical monomers were inserted perpendicularly into the upper leaflet of the membrane, the N-termini moved rapidly to the surface already during the minimization phase of the MD simulation thus bringing the gp41-FP monomers in a position similar to the one in system A2.

In Fig. 3 the time evolution of the APL and the lipid bilayer thickness d is shown during the 30 ns long MD simulations S1 and S2. While during S1 both of these quantities remained constant (i.e., APL ≈ 70 $Å^2$, and d ≈ 34 Å), in S2 as a result of the applied surface tension lead to a gradual decrease (increase) of the APL (d) to ~ 50 $Å^2$ (45 Å). According to our hypothesis that the conformational and oligomeric state of the gp41-FP is mainly determined by the APL, the dramatic reduction of the APL during S2 should lead to the destruction of the α-helical structure of the monomers A1, and their eventual transition into the more stable β-conformation at APL < 50 $Å^2$. To test this the secondary structure elements of the gp41-FP were calculated along both S1 and S2 MD trajectories by employing the STRIDE [56] algorithm as implemented in the program VMD [43] with the results shown in Fig. 4. At the beginning of the simulations S1 and S2 the α-helical regions of the A1 monomers extend only from residues 4 to 12 and 4 to 9, respectively. Note that the helical turns up to residue 16 have unwound during the minimization and equilibration process of A1 when the axes of the helices have rotated from the insertion direction (perpendicular to the membrane) to an orientation near parallel to the surface of the membrane. While during both S1 and S2 there are noticeable dynamic fluctuations in the lengths of the α-helices (colored red in Fig. 4) the trend in the structural changes of the monomers is rather different in the two cases. In S1 the α-helices are quite robust against turn- (gray regions in Fig. 4) and looser π-helix-structure (orange regions in Fig. 4) formation. Interestingly, in case of the first monomer, during 21 to 23 ns of S1 the α-helix completely disappears before it reforms again. No such refolding process has been observed during S2. In fact, during S2 the transition of the gp41-FP monomers into turn- and π-helical-structures appears to be gradual and lasting, in agreement with the hypothesis that decrease in APL does not favor the α-

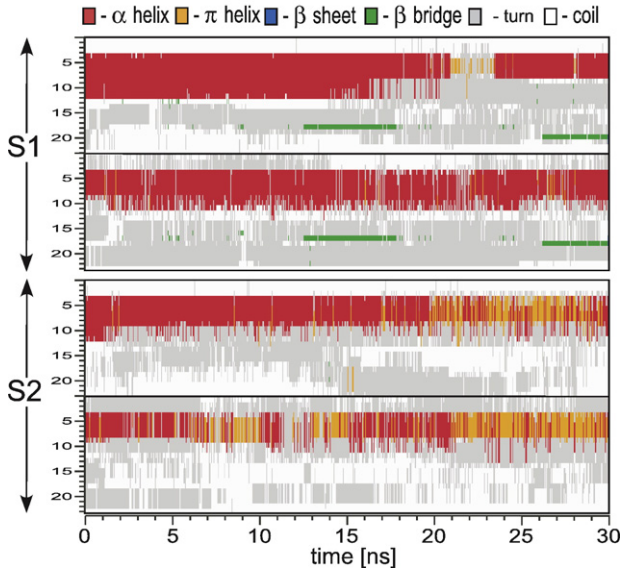

Fig. 4. Time evolution of the color coded secondary structure elements of the two gp41-FP monomers during the 30 ns long equilibrium MD trajectories S1 and S2 of system A1 described in the text. The residue numbers are on the vertical axis. In each panel the top (bottom) graph refers to the first (second) monomer. (Figure generated with the Timeline plugin of VMD [43]).

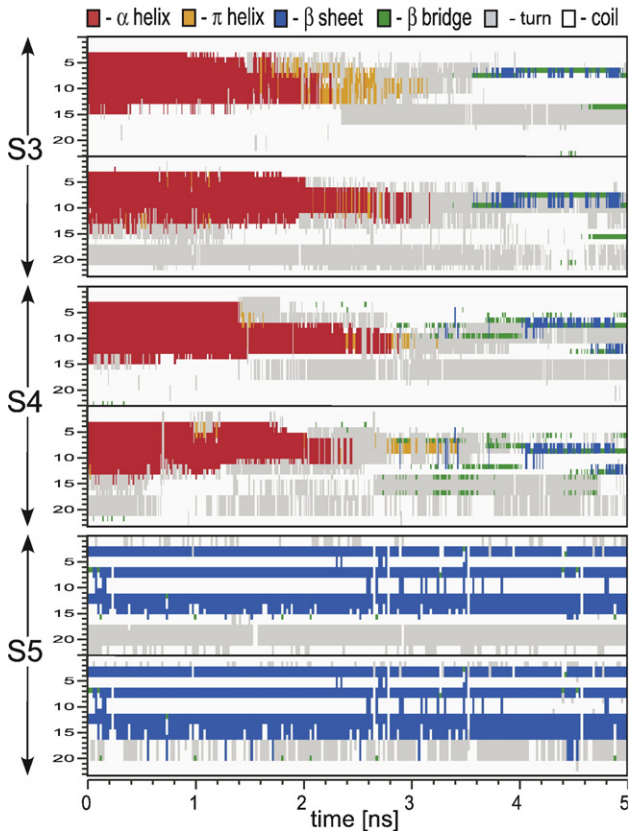

Fig. 5. Time evolution of the color coded secondary structure elements of the two gp41-FP monomers during the 5 ns long MD trajectories S3, S4 of system A2, and S5 of system B described in the text. The residue numbers are on the vertical axis. In each panel the top (bottom) graph refers to the first (second) monomer. (Figure generated with the Timeline plugin of VMD [43]).

helical structure of the gp41-FP. Furthermore, careful analysis of the S1 and S2 MD trajectories indicate that the unwinding of the α-helices are triggered by the occasional strong stochastic pulling exerted by the negative POPE phosphate group on the protonated N-terminus of the gp41-FP. Because of geometrical constraints, by decreasing the APL the rewinding of the helix becomes less favorable compared to its unwinding, thus at the end leading to the melting of the helical structure.

As already mentioned, the transition of gp41-FP from α- to β-structure in a lipid membrane occurs on a time scale that is beyond the reach of conventional MD simulation, even if a large negative surface tension is applied to mimic the reduction of the APL. In the nonequilibrium SMD simulations S3 and S4 (see Materials and methods section) the unwinding of the α-helices in the gp41-FP monomers (system A2) was accelerated by applying an elastic stretching force between $C_{\alpha 1}$ and $C_{\alpha 16}$. In addition, to mimic reduction of the APL, in case of S4 the gp41-FP monomers were pushed one towards the other by applying a constant force between the corresponding centers of mass of residues 3–9 and 10–16, respectively. The time evolution of the secondary structure elements during the 5 ns long SMD simulations S3 and S4 was monitored similarly to S1 and S2, and the results are shown in Fig. 5. Due to the applied SMD forces in both S3 and S4 it took only a few ns for the initial α-helices (red) to melt into turns (gray) followed by the emergence of β-structures (green and blue). It should be noted that a quantitative analysis of S3 and S4, as well as, their direct comparison with S1 and S2 is rather difficult because of the large irreversible perturbation exerted on the system by the SMD forces. However, a direct comparison between S3 and S4 is meaningful and can be used to provide further insight into how the decrease in APL accelerates and, therefore, favors the α- to β-structure transition in gp41-FP dimers. As shown in Fig. 5, compared to S3 in S4 the melting of the α-helices and the formation of the β-bridges and precursors of β-sheets occur faster, the latter also being more extended. Indeed, in Fig. 5 the locations of the β-structures in A2 at the end of S4 correspond to the ones in system B (gp41-FP dimer in initial β-sheet configuration) during the last 5 ns of simulation S5 described in Materials and methods section. Furthermore, the stability of the gp41-FP dimer in β-sheet structure depends crucially on the position and number of hydrogen bonds between the monomers. In particular, the separation between the corresponding β-sheet forming residues 3–4, 7–8 and 12–13 in the two monomers with parallel orientation must have well defined stable values as in case of system B. Indeed, as shown in Fig. 6 these three distances, i.e., d_{3-4}, d_{7-8} and d_{12-13}, for system B (dash-dotted lines) do not change noticeably during simulation S5 (only the last 5 ns are shown). According to Fig. 6, in system A2 the above mentioned distances converge to the optimal ones of system B only in case of S4 indicating once again that the effective reduction of the APL favors the formation of the β-structure in the gp41-FP dimer. Finally, in Fig. 7 the time evolution of the number of hydrogen bonds (counted every 10 ps and averaged over time windows of 500 ps) is shown during simulations S3, S4 and the final 5 ns of S5. While this number fluctuates around 4 in case of system B in S5, in case of system A2 increases steadily from zero to a finite value during S3 and S4. As expected, the final value of the number of

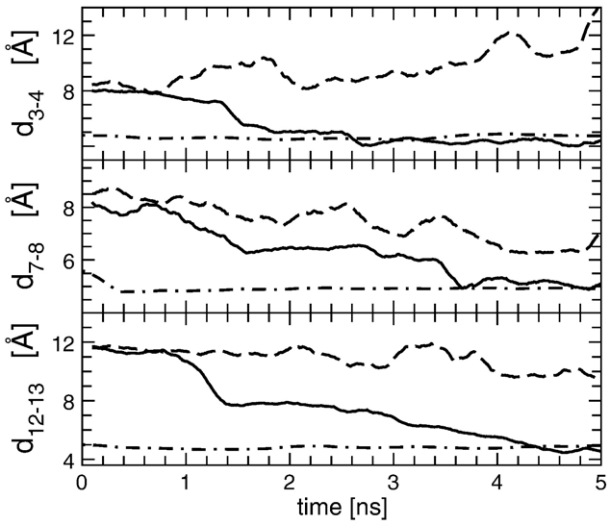

Fig. 6. Time evolution of the distance between the corresponding centers of mass of residues 3–4 (top panel), residues 7–8 (middle panel) and residues 12–13 (bottom panel) in the two gp41-FP monomers during the 5 ns SMD simulations S3 (dashed line) and S4 (solid line) of system A2 described in the text. For comparison, the time dependence of the corresponding distances in system B during simulation S5 are also shown (dash-dotted line).

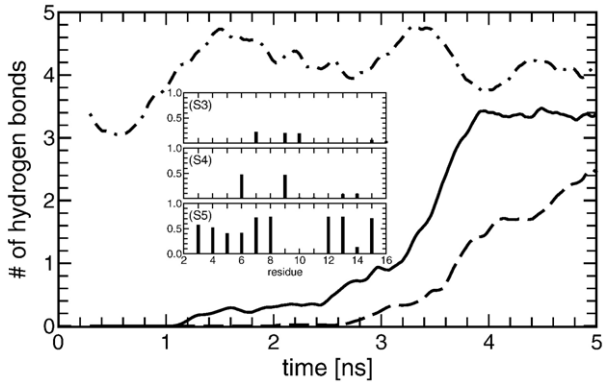

Fig. 7. Time evolution of the average number of hydrogen bonds between the two gp41-FP monomers during the MD simulations S3 (dashed line), S4 (solid line) and S5 (dash-dotted line) described in the text. Inset: Location and relative frequency distribution of the hydrogen bonds between the two gp41-FP monomers corresponding to the last 1 ns of the S3, S4 and S5 MD trajectories.

hydrogen bonds is clearly larger for S4 than in case of S3. Also, the relative frequency and location of the hydrogen bonds in A2 for S4, as shown in the inset to Fig. 7, resemble more closely to those of system B than in case of S3.

4. Discussion and conclusions

Previous structural studies of the structure of the HIV gp41 fusion peptides in membrane environments led to a variety of structures, resulting in suggestions of conformational plasticity of the FP [25,27], and its relevancy to the fusogenicity of the fusion domain. In this study, a major factor affecting the structure (and oligomeric state) adopted by the HIV gp41-FP, the surface area of the membrane or APL, has been revealed. Our hypothesis, that the structure and oligomeric state of the FP is determined by the APL of the membrane surface, and that the effects of changes in the curvature of the membrane surface on the structure of the FP are manifested by the changes in the APL, has been verified by our FTIR experiments and further corroborated by MD simulations. By using the seldom exploited AOT reversed micelles as membrane mimics in our FTIR studies, we have extended the APL range to a low value region (35–50 $Å^2$) heretofore unexplored. The extension of the APL range, from normal micelles to planar bilayers/monolayers to reversed micelles, enables us to confirm convincingly that a decrease in the APL, due to changes in curvature or due to other factors such as the addition of Ca^{++} ions [31,40] or an applied lateral pressure [39], leads to the oligomerization of the gp41-FP and the formation of β-sheet structure, while larger APL, such as in the case of normal micelles, favors monomeric helical structure. This effect may also explain the recent observations from solid-state NMR that FP monomers [57] and cross-linked trimers [58] adopt predominantly α-helical structure in POPC/POPG bilayers without cholesterol but β-strands in the presence of cholesterol. The presence of cholesterol in membrane is known to increase the lateral packing density (lower APL) and higher conformational order for the lipid chains [12,59–63]. However, the effects of direct interaction of the FP with cholesterol on the structure of the FP cannot be ruled out completely as the cause of the conformational changes observed [57,58].

The implication of the results of this work on the fusion process induced by the HIV fusion peptide is a more complicated issue. First the APL used in this study is substantially smaller than usually found in lipid bilayers. However, it is generally believed that negative curvature (and smaller APL) in cell membranes is developed during the early stage of the fusion process. In such a situation, small APL comparable to those in the current study may be achieved.

While some studies have shown that both the α-helical and β-sheet structures of the FP are fusogenic [58,64,65], results of other work suggested that specific conformation was responsible for membrane fusion [40,65]. Our findings in the present work are consistent with the conclusions of several previous studies that implicated the β-sheet structure as the fusogenic structure. It has been shown that, in the case of gp41, addition of Ca^{++} ions [40] or phosphoethanolamine lipid [66] (see also discussion later in this section) to large unilamellar vesicle promotes fusion. In both cases, the APL of the vesicle surface is reduced (although Haque et al. argued that the main effect of the addition of Ca^{++} ions is to cause vesicle aggregation [67]). In addition, it has been well established that cholesterol promotes fusion of liposomes [68] and is required in the host membrane for HIV-1 infection [69]. As discussed earlier, the presence of cholesterol increases the lateral packing density in membrane and decreases the APL. Furthermore, the longer FP constructs which adopt predominantly β-structure were found to be much more fusogenic than the shorter FPs which may adopt either α- or β-structures [32,68]. Thus, these observations appear to point to the conclusion that decreases in APL in the membrane facilitate fusion, probably by converting the FP into the β-sheet structure, which is the conformation responsible for fusion activities, as suggested earlier by Nieva et al. [40]. Such conformational "switch" and its relevance to the fusion process have been proposed for the influenza hemmaglutinin (HA) fusion peptide by Martin, et al. [70]. The Lentz group also suggested that the β-structure is the fusogenic structure in neutral lipids, although they left open the possibility of the α-helical structure as being responsible for fusion in acidic lipids [65]. It was proposed by Shai's group that the β-sheet structure would enable the N-terminal part of the gp41 fusion domain to penetrate and traverse the membrane [32] triggering the fusion process. Yet the model proposed by the Lentz group [65] has the β-structure of the gp41-FP penetrating the bilayer in a parallel (to the bilayer interface) orientation. On the other hand, early work from DeGrado's laboratory suggested that the inserted α-helical form causes vesicle membrane disruption (fusion) whereas the surface-bound β form induces aggregation of vesicles [30]. More recent work from Tamm's laboratory that included fusion studies suggested that the α-helical conformation is responsible for fusion in both HA and HIV FPs [38,71]. Martin et al. [66] showed that the HIV FP can only cause fusion in large unilamellar vesicles when phosphatidylethanolamine (PE) was present, and the orientation (oblique insertion) of the FP with respect to the membrane surface depends on the

presence of PE. PE has a much smaller APL than many other lipids, for example, PC. But yet, the conformation of the gp41-FP they determined in the presence of PE was α-helical, thus providing yet another contradiction. A most recent work by Reichert et al. [72], by introducing a single substitution of a D- or L-CF_3-phenylglycine into the gp41-FP23, contended that both the well-structured α-helical conformation and β-strand oligomeric assembly can be ruled out as the rate-determining state. Rather, fusion appears to involve conformationally disordered FPs with pronounced structural plasticity [72]. Thus, the issue of whether the α-helical or the β-sheet structure is the fusogenic structure will remain as a much-debated question.

Acknowledgments

We gratefully acknowledge the generous computational resources provided by the University of Missouri Bioinformatics Consortium. We thank Renee JiJi for the helpful discussions on the interpretation of the FTIR spectra.

References

[1] F.D. Veronese, A.L. DeVico, T.D. Copeland, S. Oroszlan, R.C. Gallo, M.G. Sarngadharan, Characterization of gp41 as the transmembrane protein coded by the HTLV-III/LAV envelope gene, Science 229 (1985) 1402–1405.
[2] D.C. Chan, D. Fass, J.M. Berger, P.S. Kim, Core structure of gp41 from the HIV envelope glycoprotein, Cell 89 (1997) 263–273.
[3] L.A. Lasky, G. Nakamura, D.H. Smith, C. Fennie, C. Shimasaki, E. Patzer, P. Berman, T. Gregory, D.J. Capon, Delineation of a region of the human immunodeficiency virus type 1 gp120 glycoprotein critical for interaction with the CD4 receptor, Cell 50 (1987) 975–985.
[4] E.A. Berger, P.M. Murphy, J.M. Farber, Chemokine receptors as HIV-1 coreceptors: roles in viral entry, tropism, and disease, Annu. Rev. Immunol. 17 (1999) 657–700.
[5] H. Choe, M. Farzan, Y. Sun, N. Sullivan, B. Rollins, P.D. Ponath, L.J. Wu, C.R. Mackay, G. LaRosa, W. Newman, N. Gerard, C. Gerard, J. Sodroski, The beta-chemokine receptors CCR3 and CCR5 facilitate infection by primary HIV-1 isolates, Cell 85 (1996) 1135–1148.
[6] B.J. Doranz, J. Rucker, Y. Yi, R.J. Smyth, M. Samson, S.C. Peiper, M. Parmentier, R.G. Collman, R.W. Doms, A dual-tropic primary HIV-1 isolate that uses fusin and the beta-chemokine receptors CKR-5, CKR-3, and CKR-2b as fusion cofactors, Cell 85 (1996) 1149–1158.
[7] T. Dragic, V. Litwin, G.P. Allaway, S.R. Martin, Y.X. Huang, K.A. Nagashima, C. Cayanan, P.J. Maddon, R.A. Koup, J.P. Moore, W.A. Paxton, HIV-1 entry into CD4(+) cells is mediated by the chemokine receptor CC-CKR-5, Nature 381 (1996) 667–673.
[8] M. Kowalski, J. Potz, L. Basiripour, T. Dorfman, W.C. Goh, E. Terwilliger, A. Dayton, C. Rosen, W. Haseltine, J. Sodroski, Functional regions of the envelope glycoprotein of human immunodeficiency virus type 1, Science 237 (1987) 1351–1355.
[9] P.A. Bullough, F.M. Hughson, J.J. Skehel, D.C. Wiley, Structure of influenza haemagglutinin at the pH of membrane fusion, Nature 371 (1994) 37–43.
[10] D. Fass, S.C. Harrison, P.S. Kim, Retrovirus envelope domain at 1.7 Angstrom resolution, Nat. Struct. Biol. 3 (1996) 465–469.
[11] W. Weissenhorn, A. Dessen, S.C. Harrison, J.J. Skehel, D.C. Wiley, Atomic structure of the ectodomain from HIV-1 gp41, Nature 387 (1997) 426–430.
[12] J.M. Smaby, M.M. Momsen, H.L. Brockman, R.E. Brown, Phosphatidylcholine acyl unsaturation modulates the decrease in interfacial elasticity induced by cholesterol, Biophys. J. 73 (1997) 1492–1505.
[13] M. Caffrey, M. Cai, J. Kaufman, S.J. Stahl, P.T. Wingfield, D.G. Covell, A.M. Gronenborn, G.M. Clore, Three-dimensional solution structure of the 44 kDa ectodomain of SIV gp41, EMBO J. 17 (1998) 4572–4584.
[14] V.N. Malashkevich, D.C. Chan, C.T. Chutkowski, P.S. Kim, Crystal structure of the simian immunodeficiency virus (SIV) gp41 core: conserved helical interactions underlie the broad inhibitory activity of gp41 peptides, Proc. Natl. Acad. Sci. U. S. A. 95 (1998) 9134–9139.
[15] Z.N. Yang, T.C. Mueser, J. Kaufman, S.J. Stahl, P.T. Wingfield, C.C. Hyde, The crystal structure of the SIV gp41 ectodomain at 1.47 Å resolution, J. Struct. Biol. 126 (1999) 131–144.
[16] K.A. Baker, R.E. Dutch, R.A. Lamb, T.S. Jardetzky, Structural basis for paramyxovirus-mediated membrane fusion, Mol. Cell 3 (1999) 309–319.
[17] W. Weissenhorn, A. Carfi, K.H. Lee, J.J. Skehel, D.C. Wiley, Crystal structure of the Ebola virus membrane fusion subunit, GP2, from the envelope glycoprotein ectodomain, Mol. Cell 2 (1998) 605–616.
[18] V.N. Malashkevich, B.J. Schneider, M.L. McNally, M.A. Milhollen, J.X. Pang, P.S. Kim, Core structure of the envelope glycoprotein GP2 from Ebola virus at 1.9-A resolution, Proc. Natl. Acad. Sci. U. S. A. 96 (1999) 2662–2667.
[19] W.R. Gallaher, Detection of a fusion peptide sequence in the transmembrane protein of human immunodeficiency virus, Cell 50 (1987) 327–328.
[20] M.D. Delahunty, I. Rhee, E.O. Freed, J.S. Bonifacino, Mutational analysis of the fusion peptide of the human immunodeficiency virus type 1: identification of critical glycine residues, Virology 218 (1996) 94–102.
[21] E.O. Freed, D.J. Myers, R. Risser, Characterization of the fusion domain of the human immunodeficiency virus type 1 envelope glycoprotein gp41, Proc. Natl. Acad. Sci. U. S. A. 87 (1990) 4650–4654.
[22] E.O. Freed, E.L. Delwart, G.L. Buchschacher, A.T. Panganiban, A mutation in the human immunodeficiency virus type 1 transmembrane glycoprotein gp41 dominantly interferes with fusion and infectivity, Proc. Natl. Acad. Sci. U. S. A. 89 (1992) 70–74.
[23] P.W. Mobley, A.J. Waring, M.A. Sherman, L.M. Gordon, Membrane interactions of the synthetic N-terminal peptide of HIV-1 gp41 and its structural analogs, Biochim. Biophys. Acta, Biomembr. 1418 (1999) 1–18.
[24] S.G. Peisajovich, R.F. Epand, M. Pritsker, Y. Shai, R.M. Epand, The polar region consecutive to the HIV fusion peptide participates in membrane fusion, Biochemistry 39 (2000) 1826–1833.
[25] S.R. Durell, I. Martin, J.M. Ruysschaert, Y. Shai, R. Blumenthal, What studies of fusion peptides tell us about viral envelope glycoprotein-mediated membrane fusion (review), Mol. Membr. Biol. 14 (1997) 97–112.
[26] J.L. Nieva, A. Agirre, Are fusion peptides a good model to study viral cell fusion? Biochim. Biophys. Acta, Biomembr. 1614 (2003) 104–115.
[27] R.M. Epand, Fusion peptides and the mechanism of viral fusion, Biochim. Biophys. Acta 1614 (2003) 116–121.
[28] J.D. Lear, W.F. DeGrado, Membrane binding and conformational properties of peptides representing the NH2 terminus of influenza HA-2, J. Biol. Chem. 262 (1987) 6500–6505.
[29] S.A. Wharton, S.R. Martin, R.W. Ruigrok, J.J. Skehel, D.C. Wiley, Membrane fusion by peptide analogues of influenza virus haemagglutinin, J. Gen. Virol. 69 (Pt 8) (1988) 1847–1857.
[30] M. Rafalski, J.D. Lear, W.F. DeGrado, Phospholipid interactions of synthetic peptides representing the N-terminus of HIV gp41, Biochemistry 29 (1990) 7917–7922.
[31] A. Saez-Cirion, J.L. Nieva, Conformational transitions of membrane-bound HIV-1 fusion peptide, Biochim. Biophys. Acta, Biomembr. 1564 (2002) 57–65.
[32] Y. Wexler-Cohen, K. Sackett, Y. Shai, The role of the N-terminal heptad repeat of HIV-1 in the actual lipid mixing step as revealed by its substitution with distant coiled coils, Biochemistry 44 (2005) 5853–5861.
[33] D.K. Chang, S.F. Cheng, V.D. Trivedi, Biophysical characterization of the structure of the amino-terminal region of gp41 of HIV-1 — implications on viral fusion mechanism, J. Biol. Chem. 274 (1999) 5299–5309.
[34] K.F. Morris, X.F. Gao, T.C. Wong, The interactions of the HIV gp41 fusion peptides with zwitterionic membrane mimics determined by NMR spectroscopy, Biochim. Biophys. Acta, Biomembr. 1667 (2004) 67–81.
[35] S. Kamath, T.C. Wong, Membrane structure of the human immunodeficiency virus gp41 fusion domain by molecular dynamics simulation, Biophys. J. 83 (2002) 135–143.
[36] C.P. Jaroniec, J.D. Kaufman, S.J. Stahl, M. Viard, R. Blumenthal, P.T. Wingfield, A. Bax, Structure and dynamics of micelle-associated human

immunodeficiency virus gp41 fusion domain, Biochemistry 44 (2005) 16167–16180.
[37] L.M. Gordon, P.W. Mobley, R. Pilpa, M.A. Sherman, A.J. Waring, Conformational mapping of the N-terminal peptide of HIV-1 gp41 in membrane environments using C-13-enhanced Fourier transform infrared spectroscopy, Biochim. Biophys. Acta, Biomembr. 1559 (2002) 96–120.
[38] Y. Li, L.K. Tamm, Structure and plasticity of the human immunodeficiency virus gp41 fusion domain in lipid micelles and bilayers, Biophys. J. 93 (2007) 876–885.
[39] S. Castano, B. Desbat, Structure and orientation study of fusion peptide FP23 of gp41 from HIV-1 alone or inserted into various lipid membrane models (mono-, bi- and multibi-layers) by FT-IR spectroscopies and Brewster angle microscopy, Biochim. Biophys. Acta, Biomembr. 1715 (2005) 81–95.
[40] J.L. Nieva, S. Nir, A. Muga, F.M. Goni, J. Wilschut, Interaction of the HIV-1 fusion peptide with phospholipid-vesicles — different structural requirements for fusion and leakage, Biochemistry 33 (1994) 3201–3209.
[41] R.A. Demel, F. Paltauf, H. Hauser, Monolayer characteristics and thermal behavior of natural and synthetic phosphatidylserines, Biochemistry 26 (1987) 8659–8665.
[42] P.L. Luisi, B.E. Straub, Reverse Micelles: Biological and Technological Relevance of Amphiphilic Structures in Apolar Media, Plenum Press, New York, 1984.
[43] W. Humphrey, A. Dalke, K. Schulten, VMD — Visual Molecular Dynamics, J. Mol. Graph. 14 (1996) 33–38.
[44] P. Grayson, E. Tajkhorshid, K. Schulten, Mechanisms of selectivity in channels and enzymes studied with interactive molecular dynamics, Biophys. J. 85 (2003) 36–48.
[45] R.B. James, C. Phillips, Wei Wang, James Gumbart, Emad Tajkhorshid, Elizabeth Villa, Christophe Chipot, Robert D. Skeel, Laxmikant Kalé, Klaus Schulten, Scalable molecular dynamics with NAMD, Journal of Computational Chemistry 26 (2005) 1781–1802.
[46] A.D. MacKerell Jr., D. Bashford, M. Bellott, et al., Self-consistent parameterization of biomolecules for molecular modeling and condensed phase simulations, FASEB J. 6 (1992) A143.
[47] A.D. MacKerell Jr., D. Bashford, M. Bellott, et al., All-hydrogen empirical potential for molecular modeling and dynamics studies of proteins using the CHARMM22 force field, J. Phys. Chem., B 102 (1998) 3586–3616.
[48] A.D. MacKerell, D. Bashford, M. Bellott, R.L. Dunbrack, J.D. Evanseck, M.J. Field, S. Fischer, J. Gao, H. Guo, S. Ha, D. Joseph-McCarthy, L. Kuchnir, K. Kuczera, F.T.K. Lau, C. Mattos, S. Michnick, T. Ngo, D.T. Nguyen, B. Prodhom, W.E. Reiher, B. Roux, M. Schlenkrich, J.C. Smith, R. Stote, J. Straub, M. Watanabe, J. Wiorkiewicz-Kuczera, D. Yin, M. Karplus, All-atom empirical potential for molecular modeling and dynamics studies of proteins, J. Phys. Chem., B 102 (1998) 3586–3616.
[49] W.L. Jorgensen, J. Chandrasekhar, J.D. Madura, R.W. Impey, M.L. Klein, Comparison of Simple potential functions for simulating liquid water, J. Chem. Phys. 79 (1983) 926–935.
[50] T. Darden, D. York, L. Pedersen, Particle mesh Ewald — an $N\cdot\mathrm{Log}(N)$ method for Ewald sums in large systems, J. Chem. Phys. 98 (1993) 10089–10092.
[51] S. Miyamoto, P.A. Kollman, Settle — an analytical version of the shake and rattle algorithm for rigid water models, J. Comput. Chem. 13 (1992) 952–962.
[52] S.E. Feller, R.W. Pastor, Constant surface tension simulations of lipid bilayers: the sensitivity of surface areas and compressibilities, J. Chem. Phys. 111 (1999) 1281–1287.
[53] J. Gullingsrud, D. Kosztin, K. Schulten, Structural determinants of MscL gating studied by molecular dynamics simulations, Biophys. J. 80 (2001) 2074–2081.
[54] B. Isralewitz, J. Baudry, J. Gullingsrud, D. Kosztin, K. Schulten, Steered molecular dynamics investigations of protein function, J. Mol. Graph. Model. 19 (2001) 13–25.
[55] S.A. Tatulian, R.L. Biltonen, L.K. Tamm, Structural changes in a secretory phospholipase A(2) induced by membrane binding: a clue to interfacial activation? J. Mol. Biol. 268 (1997) 809–815.
[56] D. Frishman, P. Argos, Knowledge-based protein secondary structure assignment, Proteins 23 (1995) 566–579.
[57] J. Yang, P.D. Parkanzky, M.L. Bodner, C.A. Duskin, D.P. Weliky, Application of REDOR subtraction for filtered MAS observation of labeled backbone carbons of membrane-bound fusion peptides, J. Magn. Reson. 159 (2002) 101–110.
[58] Z. Zheng, R. Yang, M.L. Bodner, D.P. Weliky, Conformational flexibility and strand arrangements of the membrane-associated HIV fusion peptide trimer probed by solid-state NMR spectroscopy, Biochemistry 45 (2006) 12960–12975.
[59] M. Bloom, E. Evans, O.G. Mouritsen, Physical properties of the fluid lipid-bilayer component of cell membranes: a perspective, Q. Rev. Biophys. 24 (1991) 293–397.
[60] X.M. Li, M.M. Momsen, J.M. Smaby, H.L. Brockman, R.E. Brown, Cholesterol decreases the interfacial elasticity and detergent solubility of sphingomyelins, Biochemistry 40 (2001) 5954–5963.
[61] J.R. Silvius, Role of cholesterol in lipid raft formation: lessons from lipid model systems, Biochim. Biophys. Acta. 1610 (2003) 174–183.
[62] W.H. Binder, V. Barragan, F.M. Menger, Domains and rafts in lipid membranes, Angew. Chem. Int. Ed. Engl. 42 (2003) 5802–5827.
[63] K. Simons, W.L. Vaz, Model systems, lipid rafts, and cell membranes, Annu. Rev. Biophys. Biomol. Struct. 33 (2004) 269–295.
[64] R. Yang, M. Prorok, F.J. Castellino, D.P. Weliky, A trimeric HIV-1 fusion peptide construct which does not self-associate in aqueous solution and which has 15-fold higher membrane fusion rate, J. Am. Chem. Soc. 126 (2004) 14722–14723.
[65] M.E. Haque, V. Koppaka, P.H. Axelsen, B.R. Lentz, Properties and structures of the influenza and HIV fusion peptides on lipid membranes: implications for a role in fusion, Biophys. J. 89 (2005) 3183–3194.
[66] I. Martin, F. Defrisequertain, E. Decroly, M. Vandenbranden, R. Brasseur, J.M. Ruysschaert, Orientation and structure of the NH2-terminal HIV-1 gp41 peptide in fused and aggregated liposomes, Biochim. Biophys. Acta 1145 (1993) 124–133.
[67] M.E. Haque, B.R. Lentz, Influence of gp4l fusion peptide on the kinetics of poly(ethylene glycol)-mediated model membrane fusion, Biochemistry 41 (2002) 10866–10876.
[68] A. Saez-Cirion, S. Nir, M. Lorizate, A. Agirre, A. Cruz, J. Perez-Gil, J.L. Nieva, Sphingomyelin and cholesterol promote HIV-1 gp41 pretransmembrane sequence surface aggregation and membrane restructuring, J. Biol. Chem. 277 (2002) 21776–21785.
[69] Z.H. Liao, L.M. Cimakasky, R. Hampton, D.H. Nguyen, J.E.K. Hildreth, Lipid rafts and HIV pathogenesis: host membrane cholesterol is required for infection by HIV type 1, Aids Res. Hum. Retrovir. 17 (2001) 1009–1019.
[70] E.I. Pecheur, I. Martin, A. Bienvenue, J.M. Ruysschaert, D. Hoekstra, Protein-induced fusion can be modulated by target membrane lipids through a structural switch at the level of the fusion peptide, J. Biol. Chem. 275 (2000) 3936–3942.
[71] L.K. Tamm, J. Crane, V. Kiessling, Membrane fusion: a structural perspective on the interplay of lipids and proteins, Curr. Opin. Struck. Biol. 13 (2003) 453–466.
[72] J. Reichert, D. Grasnick, S. Afonin, J. Buerck, P. Wadhwani, A.S. Ulrich, A critical evaluation of the conformational requirements of fusogenic peptides in membranes, Eur. Biophys. J. Biophys. Lett. 36 (2007) 405–413.